JOURNAL OF GEOPHYSICAL RESEARCH, VOL. 103, NO. D9, PAGES 10,697–10,711, MAY 20, 1998

Global OH trend inferred from methylchloroform measurements

Maarten Krol, Peter Jan van Leeuwen, and Jos Lelieveld

Institute for Marine and Atmospheric Research, Utrecht, Netherlands

Abstract. Methylchloroform (MCF) measurements taken at the Atmospheric Lifetime Experiment / Global Atmospheric Gases Experiment (ALE/GAGE) measurement stations are used to deduce the tropospheric OH concentration and its linear trend between 1978 and 1993. Global three-dimensional fields of OH are calculated with a transport model that includes background photochemistry. Despite the large uncertainties in these OH fields, the simulated MCF concentrations at the five ALE/GAGE stations compare reasonably well to the measurements. As a next step, the OH fields are adjusted to fit the measurements optimally. An ensemble (Monte Carlo) technique is used to optimize the OH scaling factor and to derive the linear trend in OH. The optimized OH fields and trend imply a MCF lifetime in the troposphere of 4.7 years in 1978 and of 4.5 years in 1993. For CH_4 these lifetimes (due to OH destruction only) are 9.2 and 8.6 years in 1978 and 1993, respectively. Uncertainties in these estimates are discussed using box-model calculations. The optimized OH concentration is sensitive to the strength of other MCF sinks in the model and is constrained to $1.00^{+0.09}_{-0.15} \times 10^6$ molecules cm^{-3} in 1978 and to $1.07^{+0.09}_{-0.17} \times 10^6$ molecules cm^{-3} in 1993. The deduced OH trend is sensitive to the trend in the MCF emissions and is confined to the interval between -0.1 and +1.1% yr^{-1} with a most likely value of 0.46% yr^{-1}. Possible causes of a global increase in OH are discussed. A positive OH trend is calculated due to stratospheric ozone depletion, declining CO concentrations, increased water vapor abundance, and enhanced NO_x emissions. Although the changes in the atmospheric composition are to a large extent unknown, it seems that the observed changes are consistent with significant increases in OH over the past decades.

1. Introduction

The oxidizing capacity of the atmosphere is largely determined by the OH radical. This radical is produced as a result of O_3 photolysis in the presence of water vapor:

$$O_3 + h\nu(\lambda < 320\,\text{nm}) \longrightarrow O(^1D) + O_2 \qquad (1)$$

$$O(^1D) + H_2O \longrightarrow 2\,OH \qquad (2)$$

Other mechanisms producing OH include the reaction of HO_2 with NO [e.g., *Eisele et al.*, 1997]. On a global scale the most important sink for OH is its reaction with either CO or CH_4, which are relatively well-mixed gases that limit the lifetime of OH to 1-10 s. In the planetary boundary layer, however, nonmethane hydrocarbons may be the dominant OH sink, particularly in polluted and forested areas. The lifetimes of many trace gases, and most notably those of CH_4 and CO, are determined by the reaction with OH. In order to understand the tropospheric trends and concentrations of these gases, one needs to have detailed knowledge of the tropospheric OH distribution and its temporal variation.

Methods for measuring OH in situ in the troposphere have been developed recently. These measurements, as well as modeling studies, show that the OH concentration is highly variable in space and time [*Mount and Williams*, 1997; *Poppe et al.*, 1994]. This may be expected, since OH production is determined mainly by O_3, water vapor and UV-B radiation, which are extremely variable in the troposphere. For instance, the variability of UV-B is caused by changes in the solar zenith angle, clouds, aerosols, surface reflections, and the overhead ozone column. It is reasonable to assume that the tropospheric OH concentration on a global scale is subject to considerable variation. *Dlugokencky et al.* [1996] claim that the SO_2 that was injected by Mount Pinatubo into the lower stratosphere and upper troposphere caused substantial blocking of UV-B radiation. This may have led to lower than usual tropospheric OH concentrations; these were traced in the higher than normal CH_4 growth rates during 1991 and early 1992. On the other hand, stratospheric ozone depletion leads to more UV-B radiation in the troposphere. Since stratospheric ozone has decreased since the early 1980s and even more dramatically since the eruption of Mount Pinatubo, this may have led to increasing tropospheric OH concentrations [*Bekki et al.*, 1994; *Madronich and Granier*, 1992; *Granier et al.*, 1996].

It should be realized that the OH concentration is also a strong function of cloud abundance (via O_3 photolysis),

Paper number 98JD00459.
0148-0227/98/98JD-00459$09.00

water vapor, O_3 and NO_x. Therefore, possible trends and variability in these quantities are also affecting OH concentrations. Nevertheless, stratospheric ozone depletion is held partly responsible for the rapid decline in the CO and CH_4 growth rates during 1992 and 1993 [*Bekki et al.*, 1994] (following the increases in 1991 and early 1992).

Since reaction with OH is the most important sink for CH_4, measurements of CH_4 can be used to estimate the globally averaged OH concentration. This requires detailed knowledge of the CH_4 sources. Since methane is emitted by many anthropogenic and natural sources, estimates of the total source are rather uncertain [*Prather et al.*, 1994].

The 1,1,1 trichloroethane (CH_3CCl_3 or methylchloroform, hereafter called MCF) is more likely to be able to constrain tropospheric OH concentrations [*Prinn et al.*, 1992, 1995]. Sources of this compound are purely anthropogenic, and it is claimed that the emissions are known with high accuracy [*Midgley and McCulloch*, 1995]. Most sources are located in the northern hemisphere (NH). For a few years now, the MCF concentrations in the troposphere have been declining. It has been suggested [*Spivakovsky et al.*, 1990, C. M. Spivakovsky, Past and future observations of CH_3CCl_3 as a constraint for the interhemispheric asymmetry in OH, submitted to Geophysical Research Letters, 1997] that the resulting decline in the latitudinal gradient can be used as an extra test of our understanding of OH.

Prinn et al. [1995] used the 1978-1994 Atmospheric Lifetime Experiment / Global Atmospheric Gases Experiment (ALE/GAGE) measurements [*Prinn et al.*, 1983a, b] to constrain the average lifetime of MCF (1000-200 hPa) to 4.6 ± 0.3 years. They also estimated the 1978-1994 trend in OH to be $0.0 \pm 0.2\%\ yr^{-1}$. These authors pointed out that the increases in the lower atmospheric OH levels, expected as a result of recent accelerated total ozone depletion, must, at least at low latitudes, be offset by other factors. *Prinn et al.* [1995] used a coarse-grid two-dimensional model in which the OH concentration was estimated using the MCF measurements. There has been some dispute about several aspects of the method [*Spivakovsky et al.*, 1990; *Hartley and Prinn*, 1991; *Spivakovsky et al.*, 1991; *Cunnold and Prinn*, 1991; *Spivakovsky*, 1991]. The inverse methods of *Prinn et al.* [1995] focus on the measured temporal trends, global content, and latitudinal distributions of MCF. *Spivakovsky* [1991] states that these methods are not truly independent and that the determination of both the MCF lifetime and a calibration factor is an ill-posed problem because the results are sensitive to small changes in the emissions prior to 1978. The latter problem has been solved by the recalibration of the measurements reported by *Prinn et al.* [1995]. However, to our knowledge, no attempts have been made to verify the results of *Prinn et al.* [1995] by an independent modeling approach. This is the goal of this paper.

In global three-dimensional tropospheric chemistry modeling it has become common to test the calculated OH fields by simulating the MCF concentrations and comparing these with the ALE/GAGE measurements. Because of the uncertainties in the OH chemistry, rate constants, photolysis frequencies, and distribution of OH precursors and sinks, the accuracy of the calculated OH fields is limited [e.g., *Mount and Williams*, 1997]. Therefore some deviation between the measurements and the model results can be expected. For instance, *Thompson and Stewart* [1991] estimated that a typical simulation of global mean OH contains ~ 25% uncertainty due to imprecisions of the kinetics.

In this study we simulate the ALE/GAGE MCF measurements using an OH field obtained from a tropospheric photochemistry calculation with a three-dimensional transport model. In section 3 we adjust the global OH field until a best fit is obtained with the MCF measurements. We also determine the optimal linear OH trend between 1978 and 1993. An ensemble (Monte Carlo) method is used to estimate the aforementioned scaling factor and OH trend, along with their associated errors. The sensitivity of the result to assumptions made about MCF emissions and other MCF sinks is discussed in section 4, and the sensitivity of global OH is discussed in section 5. Finally, in sections 6 and 7 we discuss the results and summarize the main conclusions.

2. Method

2.1. Model Description

The time series of MCF measured since 1978 at five ALE/GAGE stations (see section 3) have been simulated with the MOGUNTIA model [*Zimmermann*, 1984; *Crutzen and Zimmermann*, 1991]. This model was originally developed at the Max-Planck-Institute (MPI) for chemistry in Mainz, FRG (Germany), but several aspects of the model have been modified. First, the advection scheme was replaced by the less diffusive up-wind scheme QUICKEST described by *Vested et al.* [1992]. The original Oort climatology [*Oort*, 1983] was replaced by European Centre for Medium Range Weather Forecasts (ECMWF) 1987 analyzed wind data. As in the original model, the advection is run with monthly averaged winds. The variability of the winds during one month is translated into diffusion coefficients by means of Lagrangian mixing timescales [*Zimmermann*, 1984].

Deep convection is parameterized by the scheme developed by *Feichter and Crutzen* [1990]. The chemistry, which is used only to derive the initial OH field, is the same as described by *Dentener and Crutzen* [1993]. It describes the background CH_4-CO-NO_x-HO_x chemistry and accounts for heterogeneous removal of NO_x by sulfate aerosol [*Dentener and Crutzen*, 1993]. The model is run for three consecutive years with the initial conditions and emissions given in Table 1. Note that nonmethane hydrocarbon chemistry is not considered. Instead, a surrogate for these emissions has been included through CO (50%) and CH_2O (50%) emissions. *Houweling et al.* [1998] show that OH concentrations are lower over the continents when more sophisticated nonmethane hydrocarbon chemistry is included. However, these changes are compensated for by higher OH over the oceans, and the calculated small net effect in OH does not influence MCF simulations [*Houweling et al.*, 1998]. Special care has

Table 1. Initial Conditions and Sources for the 3-Year Model Simulation

Species	Initial, ppb	Source, yr^{-1}	Boundary
O_3	50	473 Tg	100 hPa[a]
CH_4	1500	523 Tg	surface
CO	60	1320 Tg	surface
NO_x	0.1	31.7 Tg N	surface
		4.7 Tg N	lightning
HNO_3	0.0	fixed concentration	100 hPa[b]
CH_2O	0.0	300 Tg	surface
C_2H_6	—	13.9 Tg	as CO and CH_2O
C_3H_8	—	17.1 Tg	as CO and CH_2O

All other species are initialized with zero concentration.

[a] Accounting for downward O_3 transport from the extratropical stratosphere.

[b] According to measurements [*Murphy et al.*, 1993].

Table 2. MCF Emissions

Year	Emission	Year	Emission	Year	Emission
1951	0.1	1966	105	1981	548
1952	0.2	1967	133	1982	522
1953	0.9	1968	147	1983	536
1954	0.6	1969	156	1984	585
1955	7.5	1970	149	1985	594
1956	13	1971	170	1986	603
1957	19	1972	214	1987	623
1958	20	1973	266	1988	666
1959	29	1974	305	1989	690
1960	35	1975	309	1990	719
1961	37	1976	382	1991	636
1962	54	1977	462	1992	592
1963	55	1978	513	1993	387
1964	57	1979	511		
1965	75	1980	537		

MCF Emissions are in units of kt yr^{-1}.

been taken to treat photolysis properly, since the global OH distribution is very sensitive to ozone photolysis. Therefore three-dimensional fields of photolysis rates are calculated, taking into account the effects of clouds, stratospheric ozone columns and surface albedo [*Krol and van Weele*, 1997]. The cloud data are taken from the International Satellite Cloud Climatology Project (ISCCP) database [*Rossow and Schiffer*, 1991] for the year 1987 and the ozone is taken from the first year of Nimbus 7 Total Ozone Mapping Spectrometer (TOMS) observations [*McPeters and Labow*, 1996], processed with the version 7 algorithm. The chemistry is calculated with a 2 hour time step, and the diurnal variation in the photolysis rates is taken into account.

The transport part of the model is used to simulate the MCF distribution. Monthly averaged OH fields are adopted from the last year of the 3-year run with chemistry. The emission estimates of MCF are taken from *Prinn et al.* [1987] (1951-1969) and from *Midgley and McCulloch* [1995] (1970-1993). The subdivision of the emissions into five distinct regions is adapted from *Midgley and McCulloch* [1995]. Within each region, the emission is distributed according to the population distribution given by *Fung et al.* [1991]. Emissions prior to 1975 are distributed as in 1975. Global MCF emissions are listed in Table 2.

Tropospheric OH is the dominant sink for MCF through the reaction

$$\mathrm{MCF} + \mathrm{OH} \xrightarrow{k} \mathrm{products} \ ; \qquad k = 1.8 \times 10^{-12} \exp \frac{-1550}{T} \tag{3}$$

[*Talukdar et al.*, 1992] with T the temperature in Kelvin. Two other sinks are taken into account: an ocean sink and destruction in the stratosphere. The hydrolysis in ocean water is computed according to *Kanakidou et al.* [1995]. We account for monthly varying fields of the height of the atmospheric mixed layer (ΔZ_1), the height of the oceanic mixed layer (ΔZ_2), and the ocean temperature (T_o). The oceanic loss term is parameterized as [*Kanakidou et al.*, 1995]

$$L_o = \varepsilon \frac{H R T_o}{\Delta Z_1} \left(\Delta Z_2 k_H + \sqrt{D_2 k_H} \right) \tag{4}$$

where ε is the ocean fraction in the grid box, H is Henry's law coefficient (M atm^{-1}), R is the gas constant (0.083 atm M^{-1} K^{-1}), k_H is the hydrolysis rate (s^{-1}), and D_2 is the diffusion coefficient in the deep (non-mixed layer) ocean (1.7 cm^2 s^{-1}). The temperature dependent hydrolysis rate k_H and Henry's law coefficient H of MCF are calculated through [*McLinden*, 1989; *Gerkens and Franklin*, 1989]

$$H = \frac{1013}{133.5} \exp\left(-20.29 + 4655/T_o\right) \tag{5}$$

$$k_H = 3.1 \times 10^{-8} \exp\left(-10000\left(1/T_o - 1/298\right)\right). \tag{6}$$

T_o is given in Kelvin, and the value for H is corrected for the effect of sea salt by multiplying with a factor of 0.8 [*McLinden*, 1989]. The ocean mixed-layer depth and temperatures were obtained from the MPI Hamburg ocean model (K. Six, personal communication, 1997). The lifetime of MCF toward oceanic loss, as calculated with this parameterization, is about 83 years, which is in good agreement with the estimate of *Butler et al.* [1991].

The net flux of MCF to the stratosphere has been parameterized as a hemispheric mean and a monthly varying loss rate at the 100 hPa level [*Kanakidou et al.*, 1995]. The stratospheric loss thus represents the net effect of the outflux in the Intertropical Convergence Zone (ITCZ) and a smaller return flux into the model domain at midlatitudes. The assumed lifetime of MCF due to stratospheric destruction is about 50 years, in agreement with *Kanakidou et al.* [1995].

The MCF simulations are carried out with a timestep of 2 hours and are compared with MCF measurements on the basis of monthly averaged MCF fields. In the model, the exchange time between the NH and SH is 1.05 year, in good agreement with other estimates [*Müller and Brasseur*, 1995].

2.2. Data Treatment

It is not easy to compare model results to measurements. First, MCF concentrations in a model represent average concentrations over a grid box, whereas measurements are taken at a single location. Second, the transport in the model uses monthly averaged wind fields augmented by diffusion and convection parameterizations. This approach neglects the role of single meteorological events which may affect mean concentrations. Finally, due to the limited resolution of the model, sharp gradients in the MCF concentration are not properly resolved. Sharp gradients are expected to occur close to sources and close to the ITCZ, which forms an MCF transport barrier between the NH and the SH.

For most MCF measurement stations, however, these problems are only minor. The ALE/GAGE measurement sites are positioned in remote regions, and pollution events, caused by transport from nearby sources, can be removed by a screening procedure [*Prinn et al.*, 1992, 1995]. The monthly averaged winds are expected to blow from pollution-free wind sectors, which favors a comparison between the screened measurements and the model. Furthermore, far away from sources the MCF fields are expected to be rather smooth. Therefore one does not expect large gradients within the corresponding model grid box. In other words, the measurement stations are representative for a large tropospheric compartment [*Prinn et al.*, 1995].

Hence we directly compare the monthly averaged model results to the monthly averaged MCF measurements (nonpolluted). We simply take the model grid box in which the measurement station is located. However, two problems arise. The Ireland station (Adrigole: 52°N, 10°W, replaced in 1987 by Mace Head: 53°N, 10°W) is located exactly on an east-west boundary of a model grid. We select the grid box located west of the station because this grid cell is free of emissions and is located upwind of MCF sources (box 20°W-10°W, 50°N-60°N). The Oregon station (Cape Meares: 45°N, 124°W) is located in a grid box in which the model emits a considerable amount of MCF. Since the measurement site is positioned at the coast (i.e., upwind from these sources, assuming a steady westerly flow), we moved the emissions from the above-mentioned grid box (120°W-130°W, 40°N-50°N) one box toward the east. The other model grid boxes that are used for the comparison are as follows: Barbados (Ragged Point: 13°N, 59°W): grid box 50°W-60°W, 10°N-20°N; American Samoa (Point Matatula: 14°S, 171°W): grid box 170°W-180°W, 10°S-20°S; and Tasmania (Cape Grim: 41°S, 145°E): grid box 140°E-150°E, 40°S-50°S.

The monthly mean mixing ratios measured at the five ALE/GAGE stations are depicted in Figure 1. Obvious local MCF pollution occurring at the Ireland, Oregon, and Tasmania stations is omitted from the data. The standard deviations are also included in Figure 1 and are calculated from the concentration fluctuations during the month [*Prinn et al.*, 1992]. The solid lines correspond to a function fit to the measurements, which will be discussed later.

The latitudinal gradient and the larger standard deviation in the NH are clearly visible in Figure 1. In particular, the tropical stations show large interannual variations. These variations cannot be reproduced by our model, since we use only 1 year of analyzed wind data and a convection parameterization which does not vary from year to year. Therefore we describe the measurements with a function which effectively filters out the seasonal cycle as well as the interannual variations. We are interested in the long-term concentration of (and the linear trend in) tropospheric OH, and this function contains exactly the information needed for comparison with our model results.

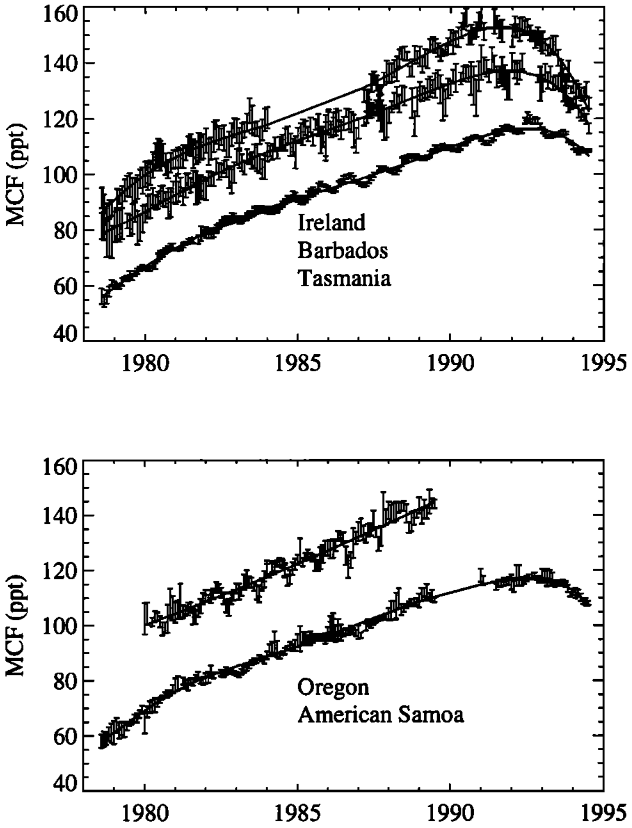

Figure 1. Monthly averaged ALE/GAGE measurements. Error bars denote 1σ variations during the month. The solid lines correspond to the function fit through the measurements (equation (7)).

Prinn et al. [1995] fitted the measurements at the five ALE/GAGE stations by means of Legendre polynomials. We follow this approach and for each station describe the MCF measurements χ by the function

$$\chi(t) = a_0 + \sum_{k=1}^{k_{\max}} N^k \frac{2^k k!}{(2k)!} a_k P_k \left(\frac{t}{N} - 1 \right) \qquad (7)$$

where N is half the length of the time series of the particular station (expressed in years), and t runs from 0 to $2N$. As a result, the argument of the Legendre function always has a value between -1 and 1. P_k corresponds to a Legendre polynomial of order k ($P_0 = 1$). The coefficients a_k in front of the Legendre function receive a proper dimension (see Table 3) by the factor in front of a_k. Here $k_{\max}$ corre-

Table 3. Optimized Legendre Coefficients Corresponding to Equation (7)

	Ireland	Oregon	Barbados	Samoa	Tasmania
Start	July/1978	Dec./1979	July/1978	July/1978	July/1978
End	Dec./1993	July/1989	Dec./1993	Dec./1993	Dec./1993
Number of points	142	124	183	170	221
a_0 (ppt)	126.7 ± 0.7	121.6 ± 0.6	114.6 ± 0.5	95.7 ± 0.4	93.9 ± 0.3
a_1 (ppt yr^{-1})	4.0 ± 0.1	4.7 ± 0.2	3.8 ± 0.1	3.7 ± 0.1	3.8 ± 0.1
a_2 (10^{-2} ppt yr^{-2})	-4.0 ± 0.8	1.2 ± 2.0	-4.6 ± 0.6	-3.7 ± 0.5	-3.5 ± 0.4
a_3 (10^{-4} ppt yr^{-3})	-9.0 ± 2		-5 ± 2	-1 ± 2	0 ± 1
a_4 (10^{-6} ppt yr^{-4})	-30 ± 5		-12 ± 4	-11 ± 3	-11 ± 3
a_5 (10^{-8} ppt yr^{-5})	-12 ± 7		-10 ± 6	-1 ± 5	-7 ± 4
a_6 (10^{-10} ppt yr^{-6})				-0 ± 7	-1 ± 5
a_7 (10^{-12} ppt yr^{-7})				-5 ± 7	

The resulting function fit is depicted in Figure 1.

sponds to the maximum order that improves the overall fit between the measurements and the functional fit still further (as measured by the sum of the squared distances between the function values and the actual measurements). The value for $k_{\max}$ differs from station to station.

The coefficients a_k are optimized by weighting each χ by the inverse of σ^2. As a consequence, the fit is less tight for the northern midlatitude and the tropical stations which experience a lot of variation during one month (see Figure 1). We include in the standard deviations an additional 5% error due to uncertainties in the absolute calibration of the MCF measurements [*Prinn et al.*, 1995]. The equation used here includes more terms than the one used by *Prinn et al.* [1995], but it does not include terms that describe a seasonal cycle. The functional fit through the measurements is depicted in Figure 1.

Table 3 lists the coefficients a_k per station and the associated 1σ errors. Note that the period over which equation (7) is evaluated is different for the Oregon station due to the different measurement period for this station. Note also that the period over which the function is evaluated runs to the end of 1993. Emission estimates for the years after 1993 were not available to us, and we prefer to compare the model and the data over the same time period.

2.3. Ensemble Method

To eliminate biases, e.g., from a single year's meteorology (1987) and systematic errors in the global mean OH calculations, we adjust the global three-dimensional OH field in order to obtain the best comparison with the ALE/GAGE measurements. In addition to adjusting the global mean OH (hereafter called ΔOH, expressed in %), we also estimate the optimal linear trend in OH (in % yr^{-1}) for the period 1978-1993. The base run is defined as the simulation with zero ΔOH and zero trend and covers the 1951-1993 period, assuming zero MCF concentrations in 1951.

ΔOH and the OH trend are varied randomly around a mean trend and ΔOH, assuming a normal distribution. To avoid excessive CPU time consumption for simulating the entire time span 1951-1993 repeatedly, the model is run for the period 1975-1993 with the initial MCF concentration taken from the base run. Errors in this initial MCF field, which are caused by errors in emissions and sinks prior to 1975, are accounted for by the introduction of a third variable. This variable, called ΔMCF (expressed in %), is also chosen randomly from a normal distribution around a mean value.

In more general terms, a vector α is defined, which contains elements which are randomly varied around a mean value. An independent model run is performed for each realization of this vector (α_i). After a number of model integrations (n), the best estimate $\tilde{\alpha}$ is obtained from a weighted average of the vectors α_i:

$$\tilde{\alpha} = \frac{\sum_{i=1}^{n} w_i \alpha_i}{\sum_{i=1}^{n} w_i}. \tag{8}$$

The associated error is given by

$$\sigma_{\tilde{\alpha}} = \sqrt{\frac{\sum_{i=1}^{n} w_i \left(\alpha_i - \tilde{\alpha}\right)^2}{\sum_{i=1}^{n} w_i}}. \tag{9}$$

After sufficient model runs, the values of $\tilde{\alpha}$ and $\sigma_{\tilde{\alpha}}$ converge to their final values. The weights w_i are a measure of how well the ith model result matches the measurements. If the match is good, a large weight is calculated, whereas a poor match leads to a low weight. Thus the weights can be interpreted as the probability of finding integration i, given the measurements and the error in the measurements. The appendix contains a more elaborate explanation of the ensemble method.

The MCF measurements are described by equation (7). This equation can also be applied to the modeled MCF concentrations. Instead of making a direct comparison between the measured and modeled MCF concentrations, we compare the coefficients of the function. The coefficients that represent the measurements are compared with the coefficients that represent the modeled MCF concentrations. When the MCF concentrations that are simulated by a model integration i are fitted to the same function, this yields the coefficients $b_{s,k,i}$ for the Legendre terms k at station s. A "penalty" function defines how well the model coefficients (mean, trend, and higher order terms) compare to the coefficients presented in Table 3. The penalty of a particular model integration i is calculated as

$$P_i = \sum_{s=1}^{5} \sum_{k=0}^{k_{\max,s}} \frac{\left(b_{s,k,i} - a_{s,k}\right)^2}{2\left(\sigma_{s,k}\right)^2} \qquad (10)$$

in which $a_{s,k}$ and $\sigma_{s,k}$ are the values given in Table 3. The model uses monthly averaged transport parameters. The variability of the modeled MCF concentrations over a month is only small and does not represent the same variability as that in the measurements. Therefore the monthly averaged model concentrations all receive equal weighting when they are fitted to equation (7).

The "global" penalty P_i of a particular model integration can be subdivided into five "station" penalties $P_{i,s}$. Penalties can be translated into weights that are required in the ensemble average of the model runs (equation (8)):

$$w_i = \exp\left(-P_i\right). \qquad (11)$$

These weights can also be calculated by using the penalties of an individual station ($P_{i,s}$). The method that has been outlined here formally corresponds to the minimum variance estimator method, assuming Gaussian error statistics (see the appendix).

In summary, the ALE/GAGE MCF measurements are represented by a function that retains only the long-term variations. The ensemble method generates model integrations with random variations in the OH trend, ΔOH, and initial MCF concentration. Subsequently, each model run is treated in the same manner as the measurements, which leads to weights that are applied to an ensemble average of the random perturbations. Finally, this ensemble average leads to optimal values for the trend, ΔOH, and initial MCF concentration, together with the associated errors.

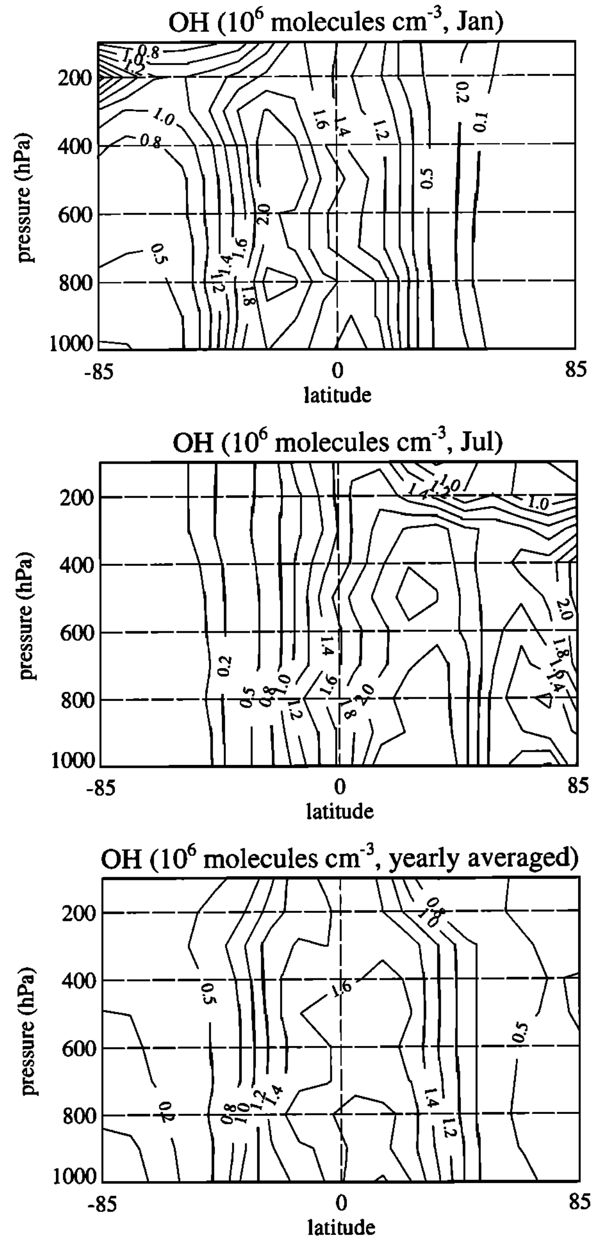

Figure 2. Zonally and 24-hour averaged OH concentrations.

3. Results

3.1. Global OH Distribution

Figure 2 displays the OH concentration obtained from the third year of a 3-year model run with chemistry. The monthly averaged OH concentrations are used in the MCF simulations. The yearly averaged field clearly shows an asymmetric OH distribution with more OH in the NH due to higher O_3 and NO_x concentrations.

Previously, OH distributions have been presented by *Kanakidou et al.* [1995], *Müller and Brasseur* [1995], *Spivakovsky et al.* [1990], and *Crutzen and Zimmermann* [1991]. These distributions all show an OH maximum in the summer hemisphere located around 800 hPa, which is more pronounced in the NH summer. If we compare our OH fields to the widely used fields of *Spivakovsky et al.* [1990], we notice that the OH concentrations generally agree well, our values being somewhat higher. Also, our maximum in the NH summer is located closer to the surface. These differences may be explained by the neglect of nonmethane hydrocarbons in our chemistry scheme. Another factor of importance is the quantum yield of the ozone photolysis (reaction (1)). In our calculations, we use the values proposed by *Michelsen et al.* [1994]. These values result in increased OH concentrations, especially in the lower troposphere due to enhanced ozone photolysis at wavelengths longer than 310 nm. Recent measurements of *Silvente et al.* [1997] indicate even higher quantum yields, which would lead to more OH in the troposphere. This is an additional uncertainty in the OH chemistry.

3.2. MCF Simulations

Figure 3 shows the 1975–1993 model-simulated MCF concentrations (base run). Although it is not the subject

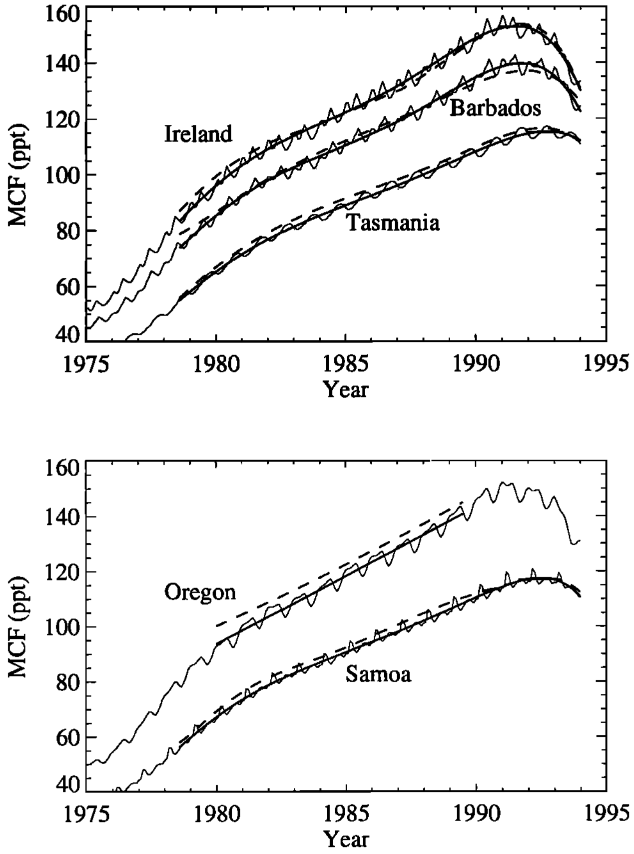

Figure 3. MCF concentration simulated at the ALE/GAGE stations by the model under base run conditions (thin line, see text). The solid lines depict the functional fit (equation (7)) through the simulated MCF concentrations. The dashed lines represent the functional fit through the measurements.

of this paper, we note that the simulated seasonal variations compare well with the measured variations. In general, the fit of the empirical function to the measurements is in fair agreement with the corresponding fit of the three-dimensional simulation. Nevertheless, in particular, for the Oregon station the model underestimates MCF concentrations. Given the large number of uncertainties in the modeling approach, however, these differences between the model and the measurements can be expected. If we try to explain the differences in terms of the OH field only (ignoring other errors in the model and input data), the comparison suggests a small overestimate of OH in the model. Also, at first sight it seems that the simulated trend differs systematically from the trend in the measurements, which suggests that these differences can be explained by imposing a trend in OH.

To determine the OH concentration and trend for which the best comparison with the measurements is obtained, we use the ensemble method outlined in section 2.3. As an example, Figure 4 shows the empirical functional fit to the first five of 200 integrations for the Samoa station. Table 4 lists the dominant penalties for these five integrations, as calculated with equation (10). The random numbers which define the integrations are drawn from the normal distributions as follows: $-5 \pm 1.4\%$ for ΔOH; $0.47 \pm 0.18\%$ yr^{-1} for the trend; and $5 \pm 7\%$ for ΔMCF.

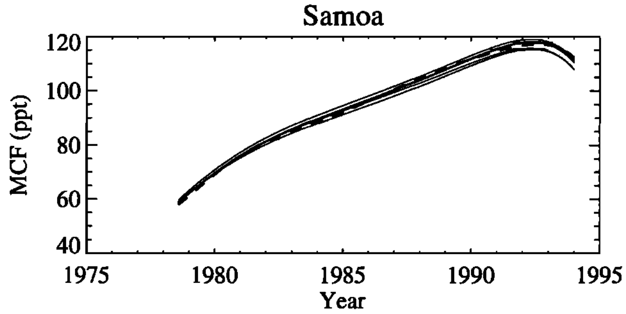

Figure 4. Solid lines are functional fit (equation (7)) through the first five MCF simulations for the Samoa station. Dashed line is corresponding fit through the MCF measurements at Samoa.

The uncertainties indicated refer to 1σ standard deviations. These distributions are rather narrow. If the distributions had been chosen wider, only a few integrations would have received a significant weight in equation (8), which would have made the method very uneconomical. Therefore pilot calculations were performed, in which the penalty function (equation (10)) was crudely minimized with respect to the three variables. As we will see later, the distributions are still wide enough for a reliable optimization of the variables.

Table 4 shows that the total penalty for this station and these integrations ranges from 1.38 to 9.87. From equation (11) it follows that the weight that is received by integration 4 is about 5000 times larger than the weight of integration 1 because the weights depend exponentially on the penalties. It is obvious that it is predominantly the lower order terms (the mean and the trend) which are sensitive to changes in the OH trend, ΔOH and ΔMCF. Higher order terms, however, may contribute significantly to the total penalty, as is shown for the P_5 term in Table 4. Note that these higher order terms do not vary strongly between the different integrations because only the global OH concentration, the trend in OH, and the initial MCF concentration are varied.

Table 5 lists the ΔOH, trend, and ΔMCF values obtained by taking an ensemble average of 200 integrations. The results are given for all stations grouped together and for the individual stations. Note that the result for all stations grouped together can be different from the average of the individual stations. Figure 5 provides a visualization of the ensemble method. In the left panels, both the initial random distributions (dotted histograms) and the final ensemble-weighted distributions are given (histogram with solid lines). The distributions are binned for this purpose. To obtain the solid line histogram, we averaged the weights of the integrations in each bin. Both distributions peak at about the same position. The weights display a narrower distribution, which confirms that the sampling has been taken from a

Table 4. Dominant Penalties Obtained for the First Five MCF Simulations for the Samoa Station

i	ΔOH, %	Trend, % yr^{-1}	ΔMCF, %	P_0	P_1	P_5	Total
1	-1.9	0.40	11.4	5.97	2.48	0.82	9.87
2	-5.9	0.50	4.6	0.47	0.07	0.83	1.63
3	-8.1	0.63	6.5	5.78	0.16	0.84	7.08
4	-5.1	0.46	6.4	0.07	0.19	0.83	1.38
5	-5.8	0.74	3.6	1.24	2.53	0.81	4.93
...							

The corresponding functional fits are displayed in Figure 4.

sufficiently wide distribution. Many of the random numbers in the tail of the initial random distributions do not contribute significantly to the final weighted average. In contrast, the three central bins of the trend histogram account for more than 60% of the total weight in the ensemble average.

The shape of the ensemble-weighted distribution reveals an anticorrelation between the trend and ΔOH. Indeed, the covariance between the trend and ΔOH is -0.88. This anticorrelation can be understood as follows. A higher trend in OH requires a smaller ΔOH value to arrive at the same average MCF destruction rate. For similar reasons, a positive covariance of 0.75 is found between ΔOH and ΔMCF.

The panels on the right-hand side of Figure 5 show the convergence of the variables as a function of the number of integrations. The vertical bars show the 1σ standard deviations. It is observed that after only about 80 integrations the ensemble average is close to the final result. However, small fluctuations remain as a result of the random nature of the estimation method. After 200 integrations, the probability is 95% that ΔOH and the OH trend are estimated with an accuracy better than 5%. For ΔMCF this accuracy is 7%. It should be stressed that these errors are purely mathematical, since model uncertainties are not considered. In the next section we will show that the errors in the variables associated with the model uncertainties are much larger than the 1σ values listed in Table 5.

Table 5 shows that the best match between the model results and the measurements is obtained if the global OH concentration is scaled down by about 5%. The ΔOH values differ between the stations and run from -3.5% to -7%. These small differences may be explained by model errors, such as a wrong OH distribution, transport errors, errors in the emission distribution, and the limited resolution. Nevertheless, it is important to note that the ΔOH value would change only by a few percent if fewer measurement stations are taken into account. For the OH trend the differences between the stations are even smaller. On the basis of each individual measurement station, a similar trend in OH is obtained. This consistent result implies that an average trend of 0.46 ± 0.09% yr^{-1} in OH has occurred on a global scale in the period 1978-1993. Another possible explanation, i.e., that the assumed trend in the MCF emissions is wrong, will be investigated in the next section. The results presented thus far have been obtained assuming that the emissions and other MCF sinks that are applied in the model are free of errors.

4. Sensitivity Analysis

To assess the sensitivity of the model to uncertainties in the sources and sinks of MCF, we condense the model into a single "global" box. The rate of change of the MCF concentration in the box is described by:

$$\begin{aligned} \frac{d\mathrm{MCF}}{dt} &= E_{\mathrm{MCF}}(t) - \mathrm{MCF} \\ &\times \left[L_{\mathrm{OH}}\left(1+\mathrm{trend}(t)\right) + L_o + L_s\right] \quad (12) \end{aligned}$$

where E_{MCF} denotes the time dependent emission (ppt yr^{-1}), and L_{OH}, L_o, and L_s (yr^{-1}) denote the MCF removal by the reaction with OH, the ocean sink, and the stratospheric destruction, respectively. These values are calculated as averages of the MCF sinks in the three-dimensional model. The OH sink is varied in time with a linear trend in the period 1978–1993. Four sensitivity runs are discussed in which the emissions and sinks of MCF are varied.

1. The stratospheric sink is increased ($1/L_s = 25$ years), the ocean sink is increased ($1/L_o = 62$ years) and the emissions are decreased by 1σ (−2.2%).

2. The stratospheric sink is decreased ($1/L_s = 75$ years), the ocean sink is decreased ($1/L_o = 134$ years) and the emissions are increased by 1σ (+2.2%).

Table 5. Ensemble-Weighted Values for ΔOH, OH Trend, and ΔMCF After 200 Integrations

Station	ΔOH, %	Trend, % yr^{-1}	ΔMCF, %
Ireland	−3.5 ± 1.0	0.44 ± 0.11	3.8 ± 5.6
Oregon	−6.9 ± 0.8	0.42 ± 0.14	11.1 ± 5.2
Barbados	−3.5 ± 0.9	0.49 ± 0.11	2.8 ± 5.5
Samoa	−5.0 ± 0.9	0.45 ± 0.10	3.4 ± 5.8
Tasmania	−5.3 ± 0.8	0.43 ± 0.09	0.8 ± 5.4
All	−4.8 ± 0.7	0.46 ± 0.09	5.5 ± 3.7

The results are given for the individual stations and for all stations grouped together (see text). Uncertainty ranges refer to 1σ.

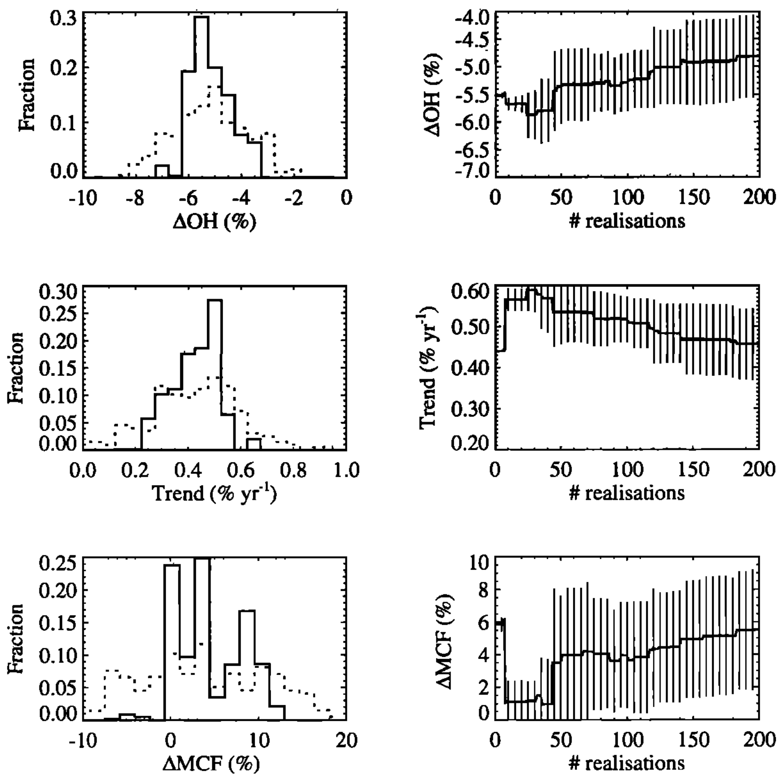

Figure 5. (left panels) Histograms of the initial normal distributions and of the ensemble-weighted distributions (see text). (right panels) Ensemble-weighted variables as a function of the number of integrations. Error bars refer to 1σ standard deviations. Top, ΔOH; middle, OH trend; bottom, ΔMCF.

3. The emission trend is increased (−4.4% in 1975 to +4.4% in 1993).
4. The emission trend is decreased (+4.4% in 1975 to −4.4% in 1993).

Thus, the MCF lifetime toward oceanic loss is varied between 62 and 134 years, according to the estimates of *Butler et al.* [1991]. The lifetime toward stratospheric loss is varied between 25 and 75 years, which is a somewhat arbitrary choice. Errors in the emission trend (runs 3 and 4) may be due to changes in unreported MCF production or to uncertainties in the translation of industrial MCF production into emission estimates [*Midgley and McCulloch,* 1995]. Following *Prinn et al.* [1992, 1995], in sensitivity run 4 (or 3) we perturb the emissions by +2σ (or −2σ) at the start of the simulation period and by −2σ (or +2σ) at the end of the simulation. These numbers are based on the differences between two emission scenarios as discussed by *Prinn et al.* [1992].

Figure 6a displays the results obtained from the box model. The ΔOH, trend, and ΔMCF values from Table 5 are used for the MCF simulations in the box model. The figure shows that the calculated MCF concentrations, averaged over the entire model domain, hardly display seasonal variations.

Figure 6b shows the perturbations of the MCF concentration for the different sensitivity runs. The first sensitivity run leads to a 9% smaller MCF burden at the end of the simulation. Since more MCF is destroyed in the stratosphere and the ocean, and less MCF is emitted, this run produces a lower bound for OH in the troposphere. The second sensitivity run mirrors this effect and produces an upper bound for OH. The OH trend calculation is expected to be sensitive to the trend in the emission estimates. For the third and fourth sensitivity runs the MCF deviations remain within 2%, with zero deviation in 1988.

Figure 6c shows the MCF perturbation for changes in the ΔOH, OH trend (T), and ΔMCF. The same box model is used, but now the terms L_{OH} and *trend* in equation (12) are perturbed as well as the initial MCF concentration.

First, ΔOH is considered. We calculate with the box model that a 10% increase in the OH concentration (from 1975 on) results in a 7% MCF reduction at the end of the simulation period. The time evolution of the perturbation matches the shape of the sensitivity runs 1 and 2 discussed above. As expected, an incorrect estimate of the MCF source, stratospheric sink, and oceanic sink can be compensated for by a change in ΔOH only.

The influence of a trend in OH on the MCF concentration differs from the ΔOH influence. If the trend in OH (i.e., 0.46% yr^{-1}) is removed, it follows that the MCF concentration increases steadily from 0% in 1978 to 5% at the end of the simulation period (Figure 6c). It is clear that the signals from sensitivity runs 3 and 4 can only be explained by

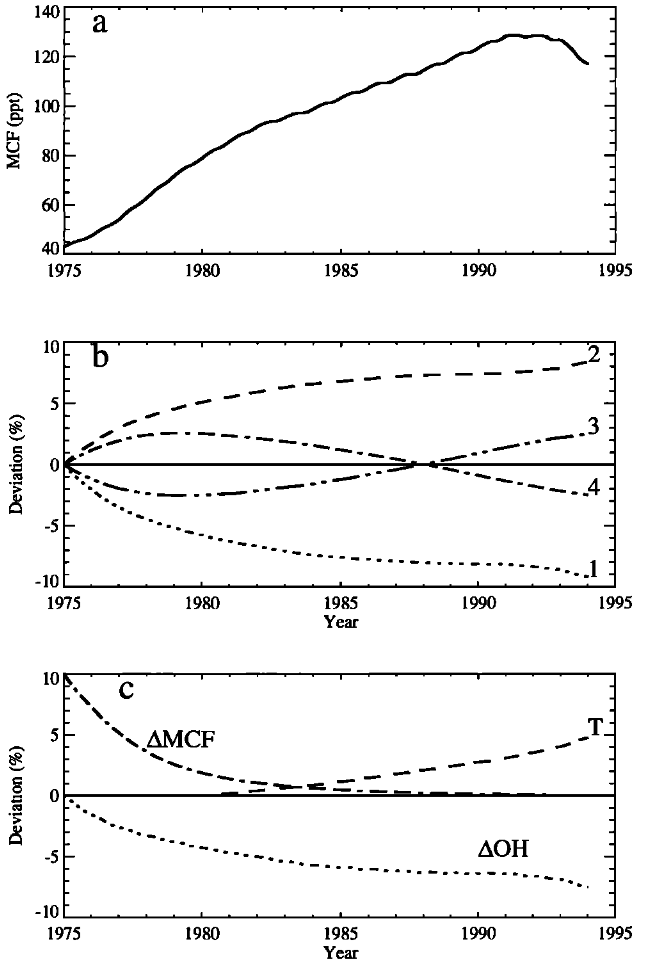

Figure 6. (a) Box model simulation of the global MCF concentration; (b) sensitivity of the global MCF concentration to the four runs (see text); (c) sensitivity of the global MCF concentration to perturbations in ΔOH, the OH trend (*T*), and ΔMCF.

adjusting the OH trend. In other words, the trend in OH is sensitive to an incorrect estimate of the emission trend. Finally, the signal from a perturbed initial MCF concentration (+10% in 1975) decays relatively rapidly. The exponential decay time equals the MCF lifetime, which is about 5 years.

Now, we return to the full three-dimensional model and reestimate ΔOH, the OH trend, and ΔMCF under the conditions of the same four sensitivity runs. The results are given in Table 6. Also given in the table are the results obtained with simulations that are based on the emissions used by *Prinn et al.* [1995]. It is shown that ΔOH runs from -19% (run 1) to +4% (run 2). As expected, these extremes occur when the perturbations of the emission and the MCF sinks all lead to a larger or smaller tropospheric MCF concentration, respectively. Consequently, significantly more (or less) OH is required to restore the agreement between the model results and the measurements.

The calculated trend in the OH concentration of 0.46% yr^{-1} vanishes when the emission trend is decreased. Alternatively, a trend of about 1% year^{-1} is found when the trend in the emission is perturbed from –4.4% in 1975 to +4.4% in 1993. The trend is much less sensitive to the perturbations applied in sensitivity runs 1 and 2. The emissions used by *Prinn et al.* [1995] result in a slightly lower trend and a less negative ΔOH value. It is unlikely that other model uncertainties (OH distribution, transport, resolution) influence the deduced OH trend. The MCF emissions assumed here therefore limit the OH trend to the interval between -0.1 and +1.1% yr^{-1}.

The results obtained for the OH trend and ΔOH would not change much when the ΔMCF value would have been kept fixed. As shown by the box model simulations, the ΔMCF perturbation diminishes at a rate that equals the MCF lifetime (about 5 years). Since we start the model runs at 1975, the low sensitivity to ΔMCF is not surprising.

Using these results, the calculated atmospheric lifetime of MCF is 4.7 ± 0.1 years in 1978 and 4.5 ± 0.1 years in 1993 (1σ errors from emission uncertainties only). This lifetime consists of a part that is determined by dissolution in the oceans (83 years), a lifetime toward stratospheric destruction (50 years), and a part that is due to oxidation by tropospheric OH (5.5 years in 1978 and 5.2 years in 1993). The MCF destruction by OH changes significantly with height. The average lifetime at the surface (1000–950 hPa) is about 3 years, whereas at 200 hPa a lifetime of almost 24 years is calculated. This is caused by the higher temperatures and OH levels close to the surface.

If the uncertainties in emissions and other MCF sinks are taken into account, the MCF lifetime toward OH oxidation is calculated to be $5.5^{+1.0}_{-0.5}$ years in 1978 (full range error). The corresponding OH number density equals $1.00^{+0.09}_{-0.15} \times 10^6$ molecules cm^{-3} (1000–100 hPa). For CH_4, these OH concentrations imply a lifetime through OH destruction of $9.2^{+1.7}_{-0.8}$ years. Owing to the trend in OH, these numbers change to $1.07^{+0.09}_{-0.17} \times 10^6$ molecules cm^{-3} and $8.6^{+1.6}_{-0.8}$ years in 1993, respectively. The uncertainties are calculated using the results of the sensitivity runs 1 and 2 listed in Table 6. In particular, the large uncertainty assumed in the stratospheric lifetime (50 ± 25 years) is responsible for the uncertainty in the global averaged OH concentration and the methane lifetime. In fact, this uncertainty in stratospheric loss may be much smaller, thus providing an upper error limit.

5. Sensitivity of the Global OH Concentration

Based on published emission estimates [*Midgley and McCulloch*, 1995; *Prinn et al.*, 1995], we infer a positive trend in OH, although we have shown that the calculated trend in OH is sensitive to the assumed trend in the emissions. Moreover, the deduced trend is almost uniform for all stations. These results thus show that the comparison between the model and the ALE/GAGE measurements improves significantly if we apply a linear trend to the global OH field. The optimized trend indicates an increase of almost 7% in the global OH concentration over the period 1978-1993. Can such a trend be explained on the basis of reasonable assumptions? To answer this question, we analyze the response of the global OH concentration in our model to several pertur-

Table 6. Ensemble-Weighted Values for ΔOH, OH trend, and ΔMCF, Obtained for the Four Sensitivity Runs (See Text) and With the Emissions Used by *Prinn et al.* [1995]

Run	ΔOH, %	Trend, % yr^{-1}	ΔMCF, %
Table 5	-4.8 ± 0.7	0.46 ± 0.09	5.5 ± 3.7
1	-19.3 ± 0.8	0.37 ± 0.10	9.6 ± 2.8
2	$+4.2 \pm 0.7$	0.44 ± 0.08	1.6 ± 2.7
3	-8.7 ± 0.7	1.08 ± 0.08	9.0 ± 3.1
4	-1.6 ± 0.7	-0.11 ± 0.07	-1.5 ± 3.2
Prinn et al. [1995]	-3.8 ± 0.8	0.42 ± 0.10	3.3 ± 4.0

The results obtained in section 3 are also given. The values refer to all stations grouped together. Uncertainty ranges refer to 1σ.

bations. It is not our goal here to make an independent estimate of the global OH changes but to investigate which factors might have contributed to a positive change in OH.

First we calculate the global OH concentrations by fixing the CH_4 and CO concentrations to the 1978 levels. Subsequently, the following six perturbations are applied.

1. The global mean CH_4 concentration in the model is increased to that observed in 1993, i.e., from 1550 ppbv to 1722 ppbv [*Schimel et al.*, 1996]. It may be expected that this contributes to an OH reduction [*Crutzen and Zimmermann*, 1991].

2. The global CO concentrations in the model are reduced to those in 1993. *Khalil and Rasmussen* [1994] and *Novelli et al.* [1994] report a rapid decline of atmospheric CO up to 8% yr^{-1} since 1990. However, during the early 1980s an increase of almost 1% yr^{-1} was observed in the midlatitude NH, while no trends could be detected in the SH [*Zander et al.*, 1989; *Brunke et al.*, 1990]. In our sensitivity study we adopt a global CO decrease of 6.5% over the 1978–1993 period.

3. The photolysis rates are recalculated to account for stratospheric ozone depletion, hence increased UV penetration into the troposphere and consequent enhancement of OH through reactions (1) and (2). The stratospheric ozone losses observed by the TOMS satellite instrument (version 7 data) are used to calculate latitudinal and height dependent trends in the photolysis rates [*De Winter-Sorkina*, 1997]. Tropospheric photolysis rate perturbations occur predominantly at higher latitudes during spring.

4. Temperatures in the model lower atmosphere are increased over the 1978-1993 period by 0.2°C based on meteorological observations. Although it is very difficult to isolate the anthropogenic signal from the large natural variability, these temperature anomalies are expected to be at least partly caused by the global warming effect of increasing greenhouse gases [*Schimel et al.*, 1996]. Increasing temperatures are expected to be accompanied by increasing water vapor concentrations, which are calculated from the change in water vapor saturation pressure.

5. Water vapor increases have been observed over the oceans, which may in part be due to increasing wind velocities [*Nicholls et al.*, 1996]. In fact, water vapor increases as high as 13% $decade^{-1}$ have been observed in the tropics [*Gaffen et al.*, 1992], which is likely to be important for OH formation through reactions (1) and (2). Here we apply an overall 10% water vapor increase in the tropics (30°N – 30°S).

6. The model OH levels appear to be very sensitive to the abundance of NO_x. Increasing NO_x enhances both the formation of ozone and the recycling of OH radicals [*Van Dop and Krol*, 1996; *Eisele et al.*, 1997]. Since reports of trends in tropospheric ozone concentrations are sparse and sometimes ambiguous [*Logan*, 1994], we prefer not to perturb the calculated ozone field but rather the NO_x emissions, increasing them by 10%.

Table 7. Responses of Global OH Concentrations to Perturbations in the Model

Perturbation (See Text)	OH Change, %
1 (11% CH_4 increase)	-1.1
2 (6.5% CO decrease)	+1.7
3 (stratospheric ozone loss)	+2.0
4 (0.2°C temperature increase)	+0.1
5 (10% tropical H_2O increase)	+1.7
6 (10% NO_x emission increase)	+2.0
7 (simultaneous perturbation)	+6.0

Table 7 lists the sensitivity of the global OH concentration to the various perturbations. As noted previously [*Van Dop and Krol*, 1996], the atmospheric chemistry system often acts as a negative feedback system so that the response to a perturbation is smaller than the perturbation itself. Nevertheless, we calculate that the small decrease in OH due to the CH_4 increase (–1.1%) is overcompensated by OH increases due to higher photolysis rates (+2%), higher NO_x emissions (+2%), decreased CO, and increased water vapor (both +1.7%). The temperature increase has only a minor effect on global OH. When all perturbations listed in Table 7 are applied simultaneously, we calculate a 6% net OH increase, which is close to the value of 7% we estimated from the MCF simulations.

It should be noted, however, that only a few of the assumptions in this sensitivity study are well documented (e.g., the CH_4 increase and the stratospheric ozone loss). Others have a weaker experimental basis (e.g., the increase in water vapor) and a potentially large effect on the OH concentrations. Therefore the perturbation calculations presented here should be conceived as a sensitivity analysis. It should be emphasized that changes in the global atmospheric composition since 1978 are to a large extent unknown. This is especially true for the most important region for OH, the lower troposphere in the tropics. In this region, large changes may be occurring due to biomass burning and rapidly emerging industrial activities. Nevertheless, it is shown here that observed changes in the atmospheric composition, in combination with some reasonable assumptions, are consistent with significant increases in OH over the past decades.

6. Discussion

The results that are presented here differ in some respects from those of *Prinn et al.* [1995]. The lower atmospheric lifetime (200-1000 hPa) of MCF given by *Prinn et al.* [1995] equals 4.6 ± 0.3 years, which agrees well with our estimate (1000-100 hPa, 4.7 years in 1978, 4.5 years in 1993, and 1σ error due to emission uncertainty of 0.1 year). *Prinn et al.* [1995] report a trend in OH of $0.0 \pm 0.2\%\ yr^{-1}$, whereas we constrained the OH trend to the range between -0.1 and 1.1% yr^{-1} with a most likely value of 0.46% yr^{-1}. This range was obtained by adjusting the emission trend. It is difficult to unambiguously establish the cause of the differences, but several possible reasons can be mentioned.

One possible cause is related to the model resolution. *Prinn et al.* [1995] resolve the atmosphere into 12 boxes. The OH concentrations in the boxes should therefore be representative for a very large domain. The OH concentration may vary considerably with longitude, for instance due to NO_x emissions and water vapor variability [*Kanakidou and Crutzen*, 1993; *Kanakidou et al.*, 1995]. Moreover, most MCF emissions are accompanied by NO_x emissions, which might lead to a positive correlation between OH and MCF. Also, the ALE/GAGE stations usually sample clean background air. In the model of *Prinn et al.* [1995] these measurements are compared to the concentrations in semihemispheric boxes, in which the MCF emissions also take place.

Another possible cause may be associated with the treatment of stratospheric MCF breakdown. In our model, stratospheric MCF losses are applied at the top of the model. These losses are calculated on the basis of two-dimensional model calculations [*Kanakidou et al.*, 1995]. *Prinn et al.* [1995] explicitly represent the stratosphere, although crudely resolved. The MCF destruction rate in the stratosphere, as well as the the stratosphere-troposphere exchange time, appear to significantly affect the MCF lifetime.

A third cause may be the estimation technique. *Prinn et al.* [1995] use an optimal estimation inversion technique to obtain the MCF lifetime and its linear trend. Although our method should, in principle, give comparable results (it also minimizes the differences between model simulations and measurements), differences in the methodology might give rise to different results. In particular, the functional fit of both the measurements and the model simulations differs from the method described by *Prinn et al.* [1995].

Finally, the calculated OH distribution is a possible cause of the differences. Whereas in the *Prinn et al.* [1995] model more OH is present in the SH, our tropospheric chemistry model calculates more OH in the NH due to the higher NO_x and O_3 levels, consistent with previous estimates [e.g., *Crutzen and Zimmermann*, 1991]. It is unlikely, however, that differences in the OH distribution influence the calculated OH trend. The consistency of the trends calculated for all ALE/GAGE measurement stations indicates an OH increase on a global scale. Therefore it seems that the downward trend since the start of industrialization [e.g., *Crutzen and Zimmermann*, 1991] may have reversed since the past several decades.

7. Summary and Conclusions

An ensemble (Monte Carlo) technique was used to obtain a best estimate for the global OH concentration and for the linear trend in OH between 1978 and 1993, simulated with a three-dimensional transport model for the troposphere. The OH fields were adopted from a model simulation with background CH_4-CO-NO_x-HO_x chemistry. The monthly averaged OH fields were adjusted until a best fit with the measurements was obtained. A linear trend in the OH field was also determined.

Rather fast convergence was obtained with the ensemble technique. However, it appeared that the choice of the initial random distributions from which the random variables (trend, ΔOH) are drawn is very critical.

A positive trend in OH of $0.46 \pm 0.6\%\ yr^{-1}$ was calculated (full range error). We deduced that he lifetime of MCF in the troposphere (1000-100 hPa) has changed from 4.7±0.1 years in 1978 to 4.5±0.1 years in 1993 (1σ error includes only the uncertainty in emissions). The corresponding global mean OH number densities indicate increases from $1.00^{+0.09}_{-0.15} \times 10^6$ molecules cm^{-3} in 1978 to $1.07^{+0.09}_{-0.17} \times 10^6$ molecules cm^{-3} in 1993. The calculated methane lifetime due to destruction by OH in the same domain (1000-100 hPa) decreases from $9.2^{+1.7}_{-0.8}$ years in 1978 to $8.6^{+1.6}_{-0.8}$ years in 1993. The errors now also include the uncertainties in the stratospheric and ocean MCF sinks. The error range adopted for the MCF lifetime due to stratospheric loss (50±25 years) is particularly large and leads to relatively large uncertainties in the OH number density and methane lifetime. These error ranges are therefore considered to be full range errors.

The estimated OH trend is sensitive to the trend in MCF emission estimates. If the trend is perturbed by –4.4% at the start of the simulation and by +4.4% at the end of the simulation, the calculated OH trend increases to 1.1% yr^{-1}. If the trend is perturbed in the opposite direction, however, the calculated trend vanishes. This indicates that the OH trend calculation depends critically on the applied MCF emission trend. Simple box model calculations support this conclusion. The estimated trend in OH is expected to be insensitive to other model uncertainties and is consistent for all measurement stations.

The optimized OH trend suggests therefore a global increase in OH of almost 7% over the period 1978-1993. A sensitivity analysis with our global chemistry model shows that reasonable assumptions about global emission estimates and the model boundary conditions are consistent with a significant increase in OH. *Prinn et al.* [1995] estimated a zero trend in OH over the same period. Since we used the same emission data, the different results must be due to the modeling approach. Other inverse modeling studies on the MCF data are required before definite conclusions about an OH trend can be drawn.

Appendix: Ensemble Method

The data-assimilation method used here is a so-called ensemble smoother. The lifetime of MCF is about 4.5 years. Therefore, the present-day MCF concentration depends on the OH concentration of the past few years. A smoother method is an inverse method that accounts for this dependence. An ensemble method uses statistical Monte Carlo methods to estimate the probability density of the model evolution.

Van Leeuwen and Evensen [1996] showed that data assimilation essentially combines the probability densities of a model and measurement data [see also *Tarantola*, 1987; *Lorenc*, 1988]. The resulting probability density contains information about both the model and the data. The essential point is that measurement data are not considered as isolated points defining the "truth" but as a particular realization from a probability distribution.

The probability density of the model evolution (the distribution follows from model uncertainties) is defined as $f(\psi)$. Using Bayes' theorem, the combined probability density of the model given the MCF measurements can be written as [see *Van Leeuwen and Evensen*, 1996]

$$f(\psi|\mathrm{d}) = \frac{f(\psi)f(\mathrm{d}|\psi)}{\int f(\psi)f(\mathrm{d}|\psi)\, d\psi} \qquad \text{(A1)}$$

In this equation, $f(\mathrm{d}|\psi)$ is defined as the probability density of the data, given a particular model integration. If we assume that the probability density of the data is Gaussian distributed, we obtain

$$f(\mathrm{d}|\psi) = A \exp\left[-\frac{(\mathrm{d}-\psi)^2}{2\sigma_{\mathrm{d}}^2}\right] \qquad \text{(A2)}$$

in which ψ denotes the model integration and σ_{d} is the measurement error. A is a normalization constant. Note that this probability density is simply Gaussian distributed around the model integration ψ.

One is generally not interested in the complete probability density $f(\psi|\mathrm{d})$, but only in its first few moments. These can be obtained by using a frequency interpretation of the probability density $f(\psi)$. For instance, the minimal variance estimate of $f(\psi|\mathrm{d})$ is the mean of this probability density, given by

$$\tilde{\psi} = \frac{\int \psi f(\psi) f(\mathrm{d}|\psi) d\psi}{\int f(\psi) f(\mathrm{d}|\psi) d\psi} = \frac{\sum_{i=1}^{N} \psi_i f(\mathrm{d}|\psi_i)}{\sum_{i=1}^{N} f(\mathrm{d}|\psi_i)} \qquad \text{(A3)}$$

Its variance can be obtained as

$$\sigma_{\tilde{\psi}}^2 = \frac{\sum_{i=1}^{N} \left(\psi_i - \tilde{\psi}\right)^2 f(\mathrm{d}|\psi_i)}{\sum_{i=1}^{N} f(\mathrm{d}|\psi_i)} \qquad \text{(A4)}$$

This frequency description of the first two moments of $f(\psi|\mathrm{d})$ is obtained from an ensemble of N model runs in a Monte Carlo simulation.

Returning to the specific example discussed in this paper, equations (A3), (A4), and (A2) correspond to equations (8), (9) and (11) in section 2.3.

Acknowledgments. We thank Sander Houweling and Frank Dentener for their helpful advice and Maria Kanakidou for the oceanic MCF removal code. We thank Ron Prinn and Xuepeng Zhao for providing their MCF emissions estimates. We thank the Carbon Dioxide Information Analysis Center for the ALE/GAGE MCF measurements. This research was supported by Space Research Organization Netherlands. P. J. van Leeuwen was supported by the National Research Program (NOP II) grant 951237.

References

Bekki, S., K. S. Law, and J. A. Pyle, The effect of ozone depletion on atmospheric CH_4 and CO concentrations, *Nature*, *371*, 595–597, 1994.

Brunke, E.-G., M. E. Scheel, and W. Seiler, Trends of tropospheric carbon monoxide, nitrous ozide and methane as observed at Cape Point, South Africa, *Atmos. Environ.*, *24A*, 585–595, 1990.

Butler, J., J. Elkins, T. Thompson, B. Hall, T. Swanson, and V. Koropalov, Oceanic consumption of CH_3CCl_3: Implications for tropospheric OH, *J. Geophys. Res.*, *96*, 22,347–22,355, 1991.

Crutzen, P. J., and P. H. Zimmermann, The changing chemistry of the troposphere, *Tellus*, *43AB*, 136–151, 1991.

Cunnold, D. M., and R. G. Prinn, Comment on "Tropospheric OH in a three-dimensional chemical tracer model: An assessment based on observation of CH_3CCl_3" by Spivakovsky et al., *J. Geophys. Res.*, *96*, 17,391–17,393, 1991.

Dentener, F. J., and P. J. Crutzen, Reaction of N_2O_5 on tropospheric aerosols: Impact on the global distributions of NO_x, O_3, and OH, *J. Geophys. Res.*, *98*, 7149–7163, 1993.

De Winter-Sorkina, R., Impact of ozone layer depletion on tropospheric ozone photodissociation rates, in *Proceedings of the Third Conference on Atmospheric Chemistry*, pp. 118–127, Am. Meteorol. Soc., Boston, Mass., 1997.

Dlugokencky, E. J., E. G. Dutton, P. C. Novelli, P. P. Tans, K. A. Masarie, K. O. Lanz, and S. Madronich, Changes in the CH_4 and CO growth rates after the eruption of Mt. Pinatubo and their link with changes in tropical tropospheric UV flux, *Geophys. Res. Lett.*, *23*, 2761–2763, 1996.

Eisele, F. L., G. H. Mount, D. Tanner, A. Jefferson, R. Shetter, J. W. Harder, and E. J. Williams, Understanding the production and interconversion of the hydroxyl radical during the Tropospheric

OH Photochemistry Experiment, *J. Geophys. Res.*, *102*, 6457–6465, 1997.

Feichter, J., and P. J. Crutzen, Parameterisation of deep cumulus convection in a global tracer transport model and its evaluation with ^{222}Rn, *Tellus*, *42B*, 100–117, 1990.

Fung, I., J. John, J. Lerner, E. Matthews, M. Prather, C. P. Steele, and P. J. Fraser, Three-dimensional model synthesis of the global methane cycle, *J. Geophys. Res.*, *96*, 13,003–13,065, 1991.

Gaffen, D. J., W. P. Elliot, and A. Roboch, Relationships between tropospheric water vapor and surface temperature as observed by radiosondes, *Geophys. Res. Lett.*, *19*, 1839–1842, 1992.

Gerkens, R. R., and J. A. Franklin, The rate of degradation of 1,1,1 trichloroethane in water by hydrolysis and dechlorination, *Chemosphere*, *19*, 1929–1937, 1989.

Granier, C., J.-F. Müller, S. Madronich, and G. P. Brasseur, Possible causes for the 1990–1993 decrease in the global tropospheric CO abundances: A three-dimensional sensitivity study, *Atmos. Environ.*, *30*, 1673–1682, 1996.

Hartley, D., and R. Prinn, Comment on "Tropospheric OH in a three-dimensional chemical tracer model: An assessment based on observation of CH_3CCl_3" by Spivakovsky et al., *J. Geophys. Res.*, *96*, 17,383–17,387, 1991.

Houweling, S., F. J. Dentener, and J. Lelieveld, The impact of nonmethane hydrocarbon compounds on tropospheric photochemistry, *J. Geophys. Res.*, *in press*, 1998.

Kanakidou, M., and P. J. Crutzen, Scale problems in atmospheric chemistry modeling: Comparison of results obtained with a three-dimensional model, adopting longitudinally uniform and varying emissions of NO_x and NMHC, *Chemosphere*, *26*, 787–802, 1993.

Kanakidou, M., F. J. Dentener, and P. J. Crutzen, A global three-dimensional study of the fate of HCFCs and HFC-134a in the troposphere, *J. Geophys. Res.*, *100*, 18,781–18,801, 1995.

Khalil, M. A. K., and R. A. Rasmussen, Global decrease in atmospheric carbon monoxide concentration, *Nature*, *370*, 639–641, 1994.

Krol, M. C., and M. van Weele, Implications of variations in photodissociation rates for global tropospheric chemistry, *Atmos. Environ.*, *31*, 1257–1273, 1997.

Logan, J. A., Trends in the vertical distribution of ozone: An analysis of ozonesonde data, *J. Geophys. Res.*, *99*, 25,553–25,585, 1994.

Lorenc, A. C., Optimal nonlinear objective analysis, *Q. J. R. Meteorol. Soc.*, *114*, 205–240, 1988.

Madronich, S., and C. Granier, Impact of recent total ozone changes on tropospheric ozone photodissociation, hydroxyl radicals, and methane trends, *Geophys. Res. Lett.*, *19*, 465–467, 1992.

McLinden, M. O., Physical properties of alternatives of the fully halogenated chlorofluorocarbons, in *Scientific Assessment of Stratospheric Ozone: 1989 WMO Report 20*, pp. 11–41, World Meteorol. Organ., Geneva, 1989.

McPeters, R. D., and G. J. Labow, An assessment of the accuracy of 14.5 years of Nimbus 7 TOMS Version 7 ozone data by comparison with the Dobson network, *Geophys. Res. Lett.*, *23*, 3695–3698, 1996.

Michelsen, H. A., R. J. Salawich, P. O. Wennberg, and J. G. Anderson, Production of $O(^1D)$ from photolysis of O_3, *Geophys. Res. Lett.*, *21*, 2227–2230, 1994.

Midgley, P., and A. McCulloch, The production and global distribution of emissions to the atmosphere of 1,1,1, trichloroethane (methyl chloroform), *Atmos. Environ.*, *29*, 1601–1608, 1995.

Mount, G. H., and E. J. Williams, An overview of the tropospheric OH Photochemistry Experiment, Fritz Peak / Idoha Hill, Colorado, fall 1993, *J. Geophys. Res.*, *102*, 6171–6186, 1997.

Müller, J.-F., and G. Brasseur, IMAGES: A three-dimensional chemical transport model of the global troposphere, *J. Geophys. Res.*, *100*, 16,445–16,490, 1995.

Murphy, D. M., D. W. Fahey, M. H. Proffitt, S. C. Liu, K. R. Chan, C. S. Eubank, S. R. Kawa, and K. K. Kelly, Reactive nitrogen and its correlation with ozone in the lower stratosphere and upper troposphere, *J. Geophys. Res.*, *98*, 8751–8773, 1993.

Nicholls, N., G. V. Gruza, J. Jouzel, T. R. Karl, L. A. Ogallo, and D. E. Parker, Observed Climate Variability and Change, in *Climate Change 1995: the Science of Climate Change*, edited by J. T. Houghton et al., pp. 133–192, Cambridge Univ. Press, New York, 1996.

Novelli, P. C., K. A. Masarie, P. P. Tans, and P. M. Lang, Recent changes in atmospheric carbon monoxide, *Science*, *263*, 1587–1590, 1994.

Oort, A., Global atmospheric circulation statistics 1958-1973, NOAA Prof. Pap. 14, U.S. Gov. Print. Off., Washington, D.C., 1983.

Poppe, D., et al., Comparison of measured OH concentrations with model calculations, *J. Geophys. Res.*, *99*, 16,633–16,642, 1994.

Prather, M., R. Derwent, D. Ehhalt, P. Fraser, E. Sanhueza, and X. Zhuo, Other trace gases and atmospheric chemistry, in *Climate Change 1994: Radiative Forcing of Climate Change and an Evoluation of the IPCC IS92 Emissions Scenarios*, edited by J. T. Houghton et al., pp. 73–126, Cambridge Univ. Press, New York, 1994.

Prinn, R. G., et al., The Atmospheric Lifetime Experiment, 1, Introduction, instrumentation and overview, *J. Geophys. Res.*, *88*, 8353–8367, 1983a.

Prinn, R. G., R. A. Rasmussen, P. G. Simmonds, F. N. Alyea, D. M. Cunnold, B. C. Lane, C. A. Cardelino, and A. J. Crawford, The Atmospheric Lifetime Experiment, 5, Results for CH_3CCl_3 based on three years of data, *J. Geophys. Res.*, *88*, 8415–8426, 1983b.

Prinn, R. G., D. Cunnold, R. Rasmussen, P. Simmonds, F. Alyea, A. Crawford, P. Fraser, and R. Rosen, Atmospheric trends in methylchloroform and the global average for the hydroxyl radical, *Science*, *238*, 945–950, 1987.

Prinn, R. G., et al., Global average concentration and trend for hydroxyl radicals deduced from ALE/GAGE trichloroethane (methyl chloroform) data for 1978-1990, *J. Geophys. Res.*, *97*, 2445–2461, 1992.

Prinn, R. G., R. F. Weiss, B. R. Miller, J. Huang, F. N. Alya, D. M. Cunnold, P. J. Fraser, D. E. Hartley, and P. G. Simmonds, Atmospheric trends and lifetime of CH_3CCl_3 and global OH concentrations, *Science*, *269*, 187–190, 1995.

Rossow, W. B., and R. A. Schiffer, ISCCP cloud data products, *Bull. Am. Meteorol. Soc.*, *92*, 2–20, 1991.

Schimel, D., et al., Radiative forcing of climate change, in *Climate Change 1995: the Science of Climate Change*, edited by J. T. Houghton et al., pp. 65–131, Cambridge Univ. Press, New York, 1996.

Silvente, E., R. C. Richter, M. Zheng, E. S. Saltzman, and A. J. Hynes, Relative quantum yields for O^1D production in the photolysis of ozone between 301 and 336 nm: Evidence for the participation of a spin-forbidden channel, *Chem. Phys. Lett.*, *264*, 309–315, 1997.

Spivakovsky, C. M., Reply on the comment by D. M. Cunnold and R. G. Prinn, *J. Geophys. Res.*, *96*, 17,395–17,398, 1991.

Spivakovsky, C. M., R. Yevich, J. A. Logan, S. C. Wofsy, M. B. McElroy, and M. J. Prather, Tropospheric OH in a three-dimensional chemical tracer model: An assessment based on observations of CH_3CCl_3, *J. Geophys. Res.*, *95*, 18,441–18,471, 1990.

Spivakovsky, C. M., R. Yevich, J. A. Logan, S. C. Wofsy, M. B. McElroy, and M. J. Prather, Reply on the comment by D. Hartley and R. G. Prinn, *J. Geophys. Res.*, *96*, 17,389–17,390, 1991.

Talukdar, R. K., A. Mellouki, A. Schmoltner, T. Watson, S. Motzka, and A. R. Ravishankara, Kinetics of the OH reaction with methylchloroform, *Science*, *257*, 227–230, 1992.

Tarantola, A., *Inverse Problem Theory: Methods for Data Fitting and Model Parameter Estimation*. Elsevier, New York, 1987.

Thompson, A. M., and R. W. Stewart, Effect of chemical kinetics uncertainties on calculated constituents in a tropospheric photochemical model, *J. Geophys. Res.*, *96*, 13,089–13,108, 1991.

Van Dop, H., and M. Krol, Changing trends in tropospheric methane and carbon monoxide: A sensitivity analysis of the OH-radical, *J. Atmos. Chem.*, *25*, 271–288, 1996.

Van Leeuwen, P. J., and G. Evensen, Data assimilation and inverse methods in terms of a probabilistic formulation, *Mon. Weather Rev.*, *124*, 2898–2913, 1996.

Vested, H. J., P. Justesen, and L. Ekebjærg, Advection dispersion modelling in three dimensions, *Appl. Math. Modell.*, *16*, 506–519, 1992.

Zander, R., P. Demanlin, D. H. Ehhalt, and U. Schmidt, Secular increase of the total vertical column abundance of carbon monoxide above central Europe since 1950, *J. Geophys. Res.*, *94*, 11,021–11,028, 1989.

Zimmermann, P. H., Ein drei-dimensionales numerisch Transportmodell für atmosphärische Spurenstoffe, dissertation, Mainz Univ., Mainz, Germany, 1984.

M. Krol, J. Lelieveld, and P. J. van Leeuwen, Institute for Marine and Atmospheric Research, Utrecht, Utrecht University, Princetonplein 5, 3584 CC, Utrecht, Netherlands. (e-mail: krol@fys.ruu.nl; J.Lelieveld@fys.ruu.nl; leeuwen@fys.ruu.nl)

(Received August 5, 1997; revised January 30, 1998;
accepted February 3, 1998.)